Supplemental Figure 1

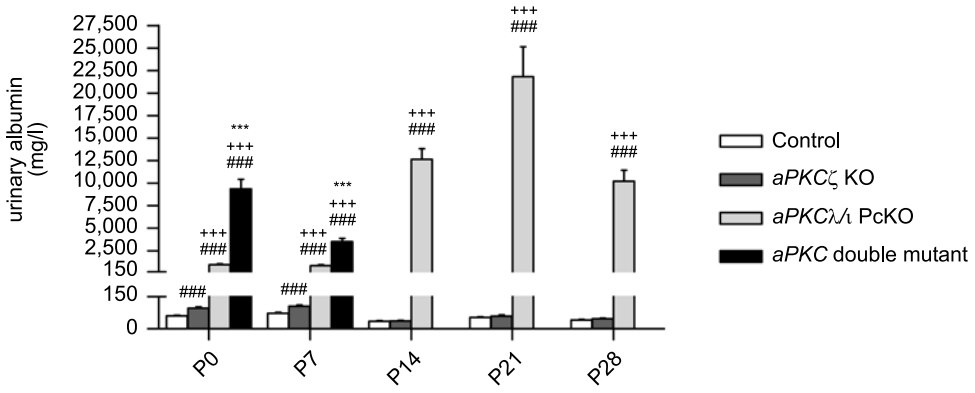

Supplemental Figure 1: Double knockout of *aPKC*λ/ι and *aPKC*ζ in podocytes results in severe albuminuria.

Follow up analysis of urinary albumin (n = 7-48 each group; * P < 0.05, ** P < 0.01, *** P < 0.001, compared to *aPKC*λ/ι PcKO; +, compared to *aPKC*ζ KO accordingly; #, compared to control accordingly). Urinary albumin concentration at P0: control 60.2 mg/l, *aPKC*ζ KO 96.3 mg/l, *aPKC*λ/ι PcKO 959.9 mg/l, *aPKC* double mutant 9,351.2 mg/l.

Supplemental Figure 2

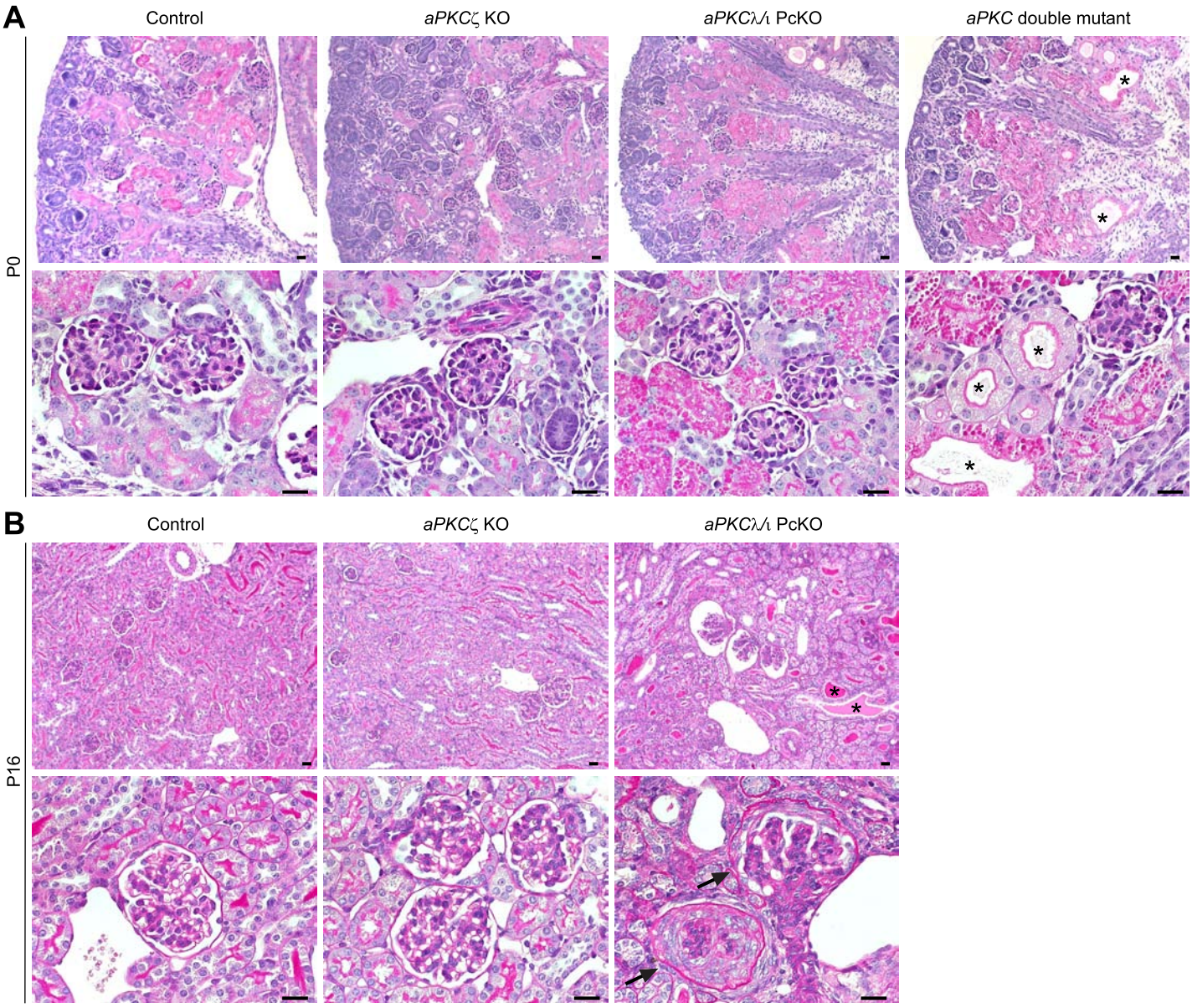

Supplemental Figure 2: Histological analysis at P0 and P16.

(A, B) PAS staining of mouse kidney sections of the genotypes as indicated. Asterisks mark tubular dilations with protein casts in kidneys of newborn *aPKC* double mutant mice (P0) and in kidneys of *aPKC*λ/ι PcKO mice at P16. Arrows mark sclerosed glomeruli. Scale bars: 20 µm.

Supplemental Figure 3

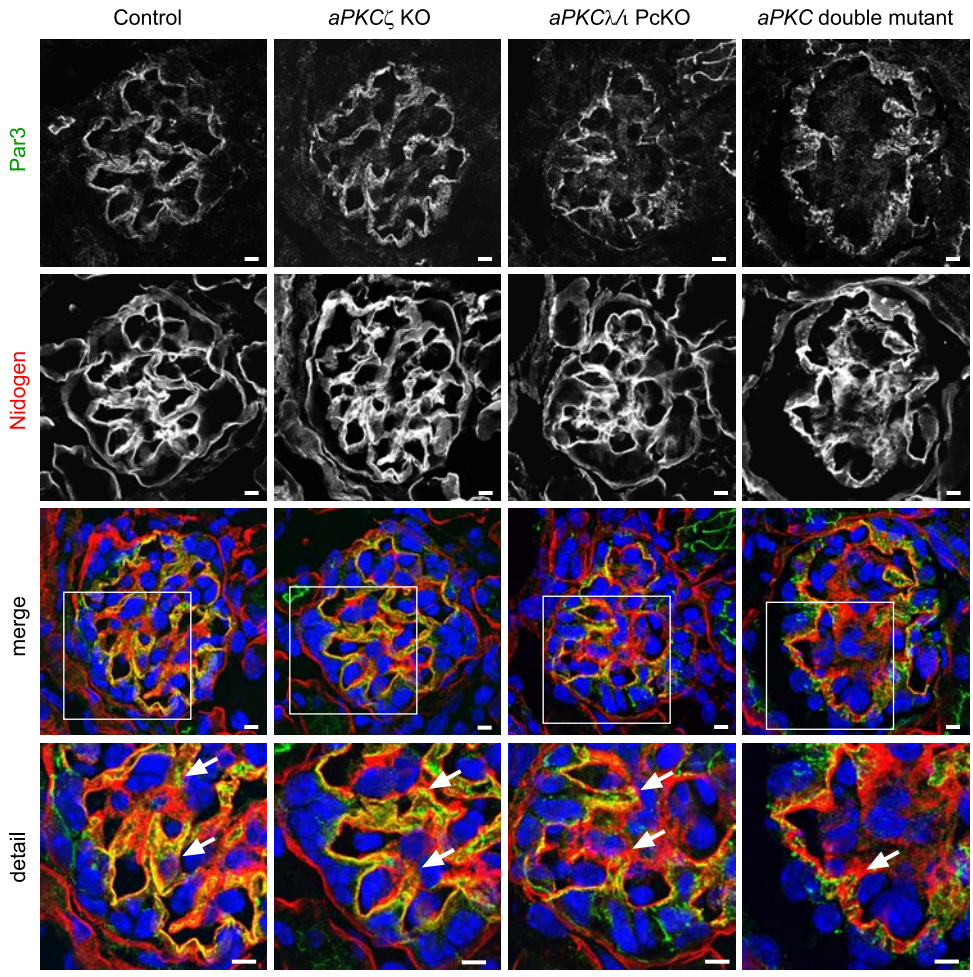

Supplemental Figure 3: Impaired glomerular infolding in *aPKC* double mutant mice.

Frozen kidney sections of newborn mice of the indicated genotypes (P0) were stained for the polarity protein Par3 and the basement membrane marker Nidogen. Arrows indicate surface invagination and enwrapping of the capillaries by the Par3 positive stained podocyte process network. In *aPKC* double mutant mice, surface infolding is severely impaired and Par3 displays a granular staining pattern. Scale bars: 5 µm.

Supplemental Figure 4

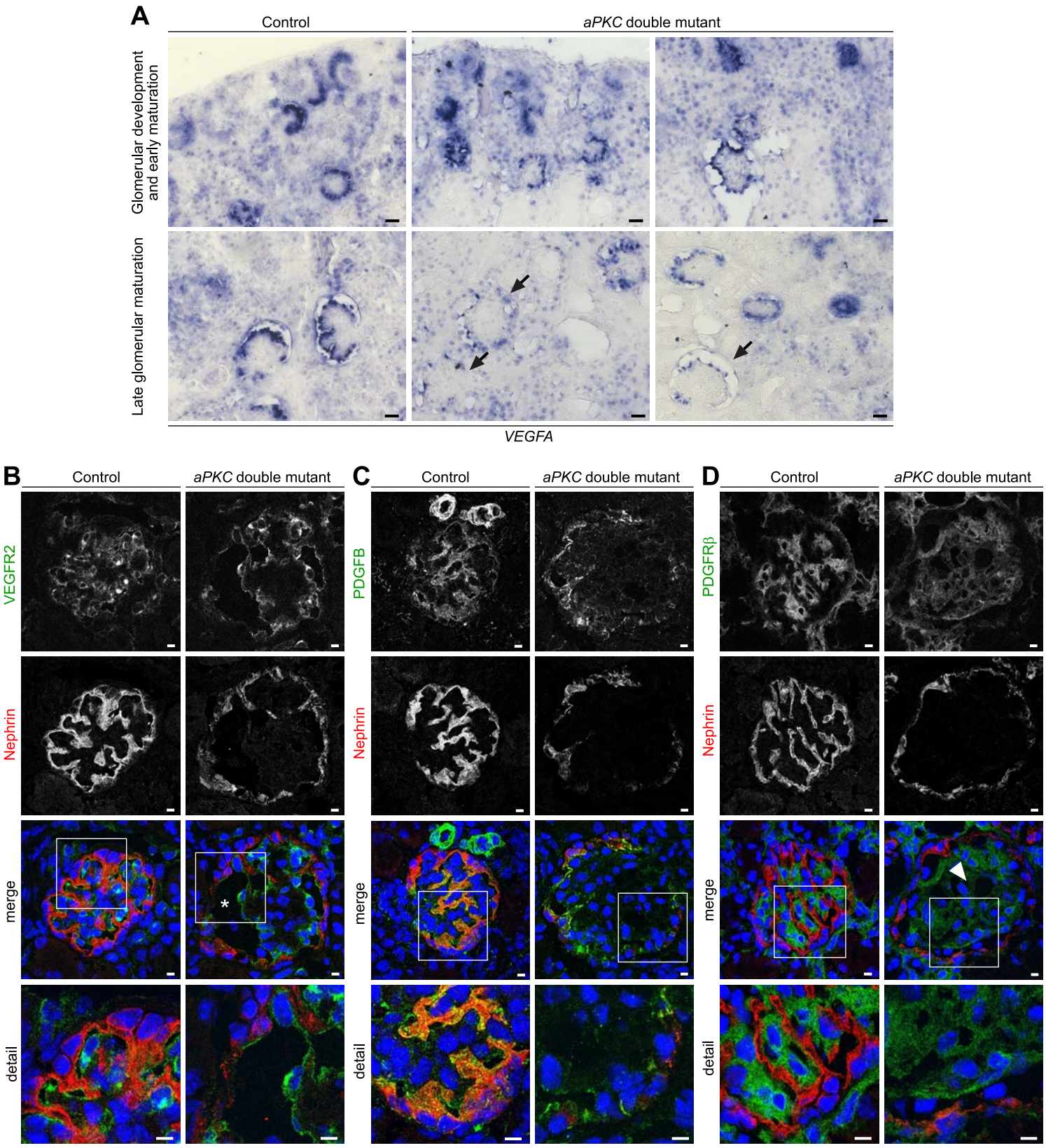

Supplemental Figure 4: Glomerular expression of VEGFA, PDGFB and their respective receptors.

(A) In situ hybridization studies of kidneys of control and *aPKC* double mutant mice at P4. During capillary loop stage and in glomeruli during early maturation no significant differences in *VEGFA* expression could be detected (upper panel), while during late maturation glomeruli of *aPKC* double mutant mice displayed reduced *VEGFA* expression (arrows, lower panel). **(B)** Frozen kidney sections of control and *aPKC* double mutant mice at P4 were stained for VEGFR2 and the podocyte marker Nephrin. Asterisk marks aneurysm. **(C, D)** Reduced PDGFB and PDGFRβ expression during late glomerular maturation at P4. Arrowhead marks mesangiolysis. Scale bars: 20 µm in A, 5 µm in B, C and D.

Supplemental Figure 5

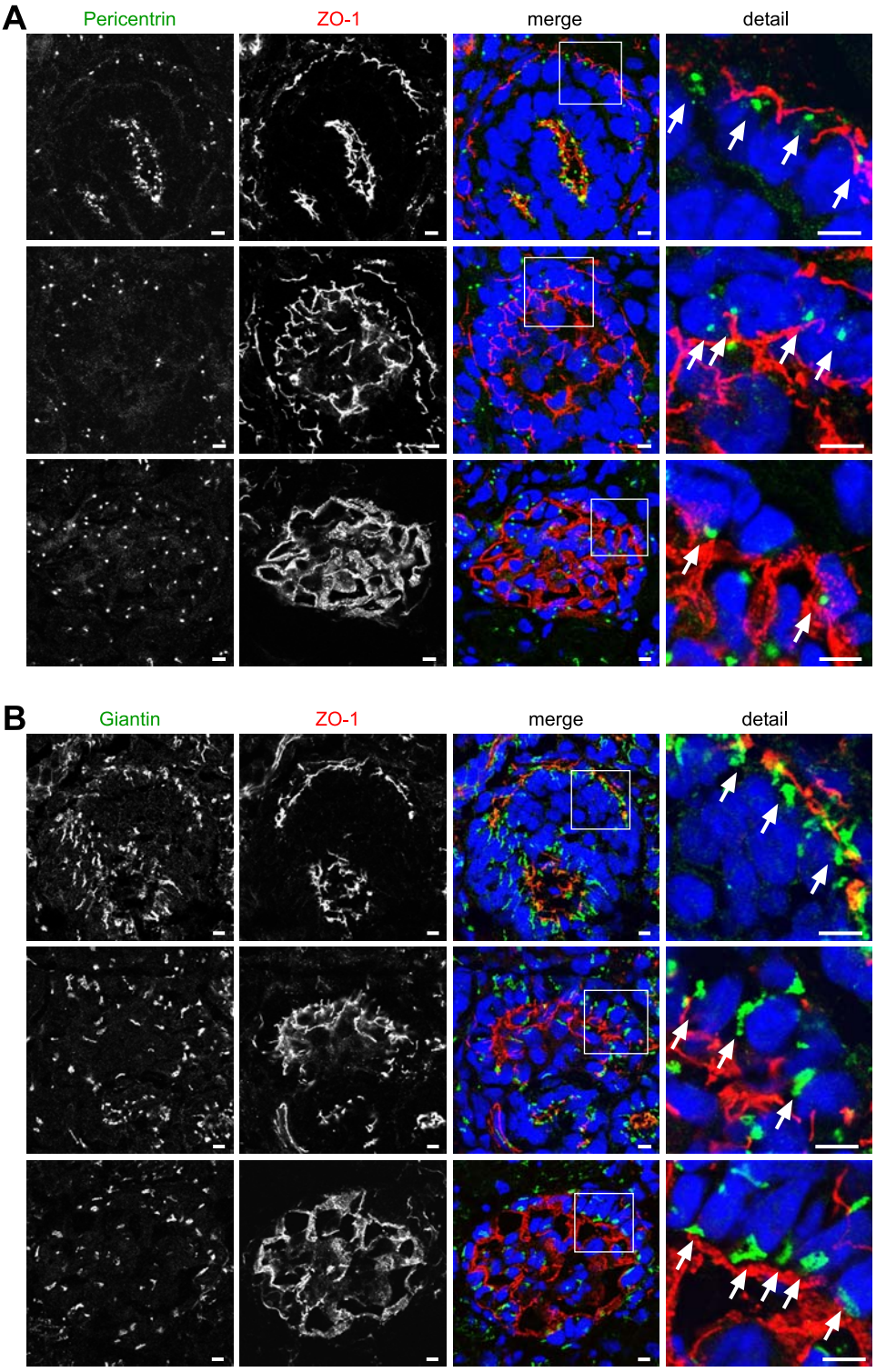

Supplemental Figure 5: Translocation of centrosome and Golgi-apparatus during podocyte differentiation in the newborn rat. Frozen kidney sections of newborn wildtype rat were stained using antibodies against the junction marker ZO-1 and **(A)** the centrosome marker protein Pericentrin (arrows) or **(B)** the Golgi-apparatus marker Giantin (arrows) respectively (developmental stages in A: top, comma-shaped body stage; middle, late s-shaped body stage; bottom, immature glomerulus; developmental stages in B: top, comma-shaped body stage; middle, late s-shaped body stage/early capillary loop stage; bottom, immature glomerulus). Scale bars: 5 µm.

Supplemental Figure 6

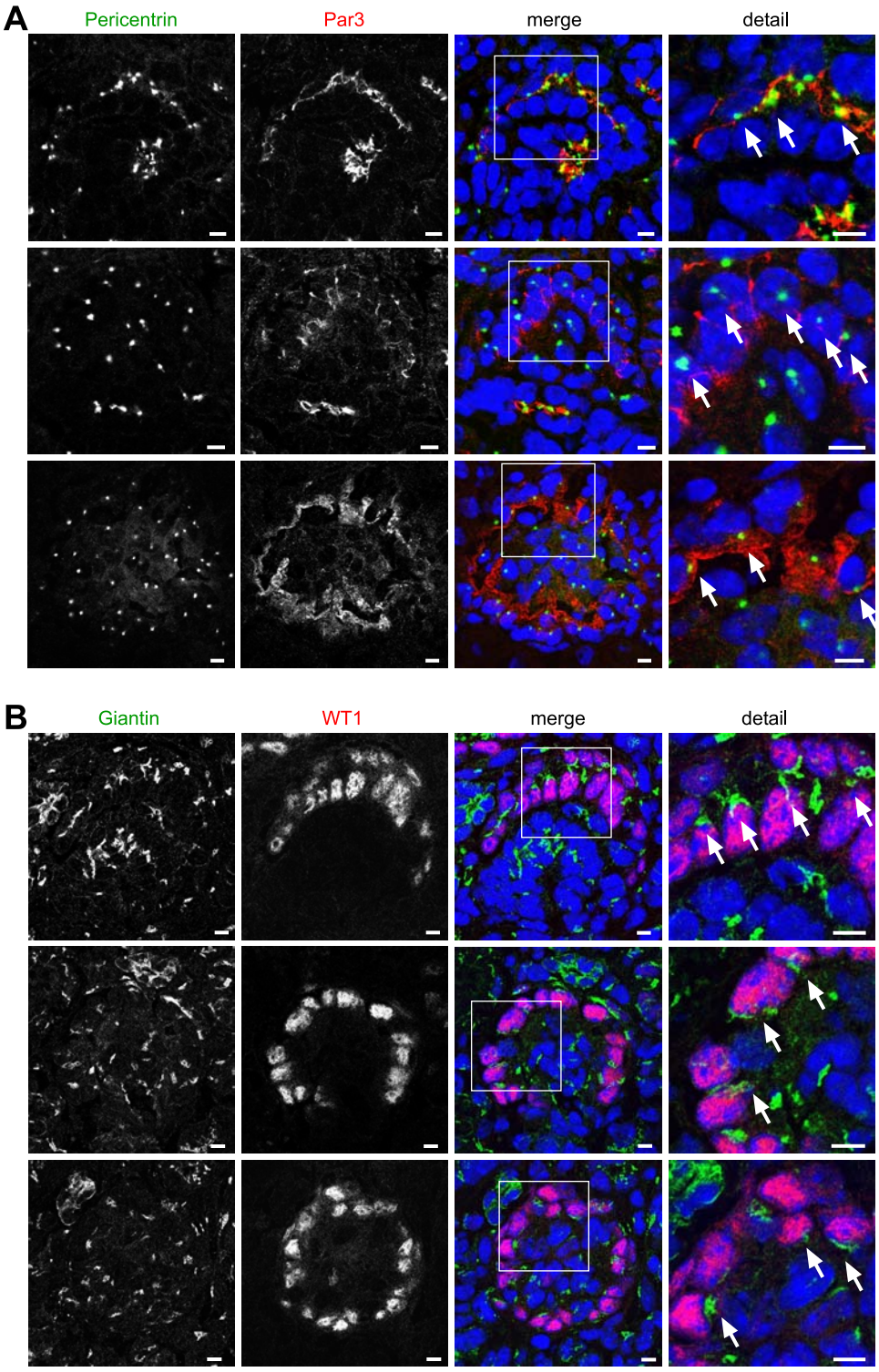

Supplemental Figure 6: Translocation of centrosome and Golgi-apparatus during podocyte differentiation in the newborn mouse. **(A)** Frozen kidney sections of newborn wildtype mice were stained using antibodies against the centrosome marker protein Pericentrin (arrows) and the polarity protein Par3 and were subjected to confocal laser microscopy (top, comma-shaped body stage; middle, s-shaped body stage; bottom, capillary loop stage). **(B)** Frozen kidney sections of newborn wildtype mice were stained using antibodies against the Golgi-apparatus marker protein Giantin (arrows) and the podocyte marker protein WT1 (top, comma-shaped body stage; middle, late s-shaped body stage/early capillary loop stage; bottom, late capillary loop stage). Scale bars: 5 µm.

Supplemental Figure 7

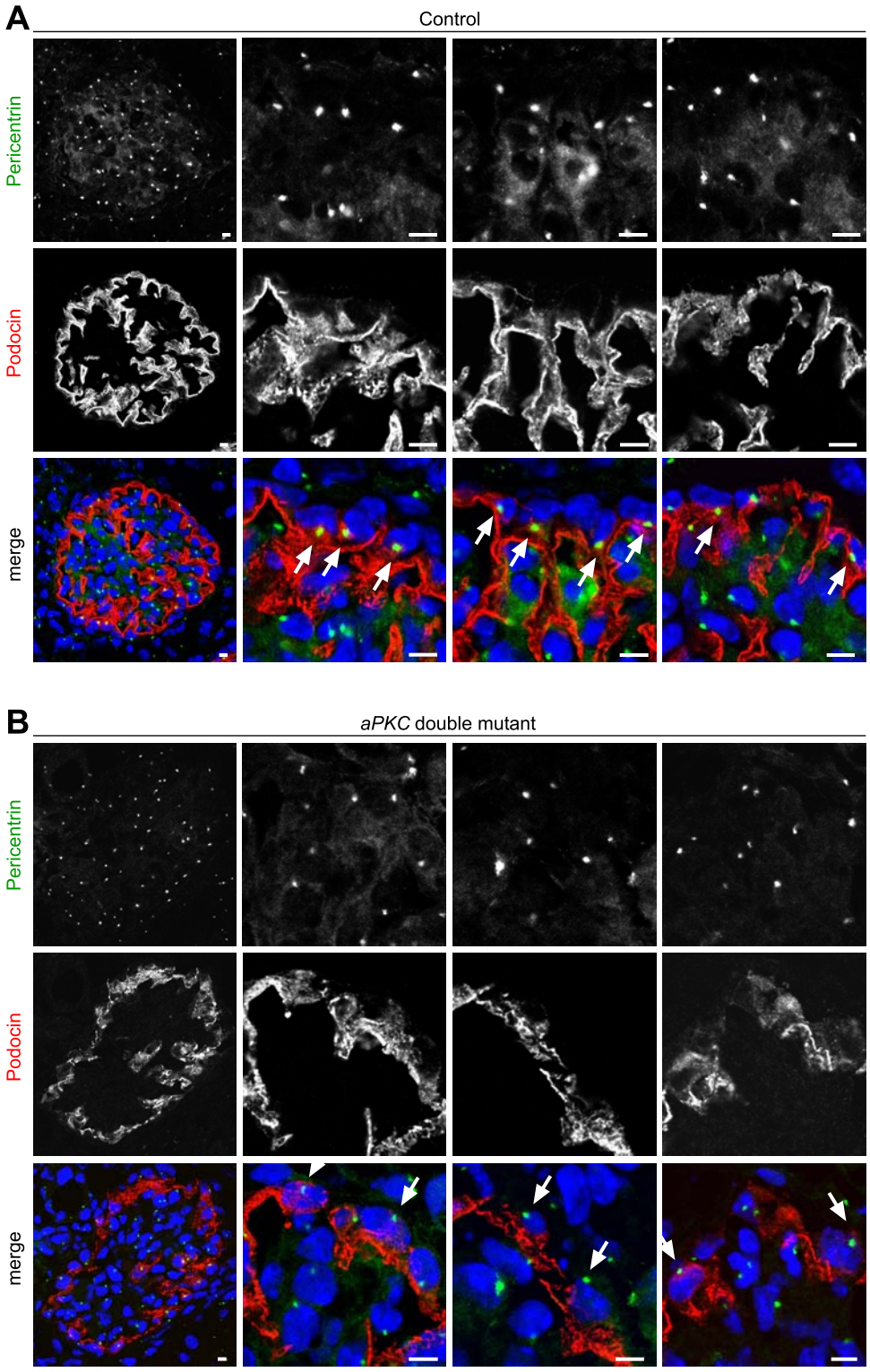

Supplemental Figure 7: Aberrant positioning of centrosomes in *aPKC* double knockout podocytes.

(A, B) Frozen kidney sections of control and *aPKC* double mutant mice at P4 were stained for the centrosome marker Pericentrin and the podocyte marker Podocin. While in control mice centrosomes (arrows) are restricted to the basal pole of the cytoplasm, in *aPKC* double knockout podocytes aberrant localization (arrows) can be detected. Scale bars: 5 µm.

Supplemental Figure 8

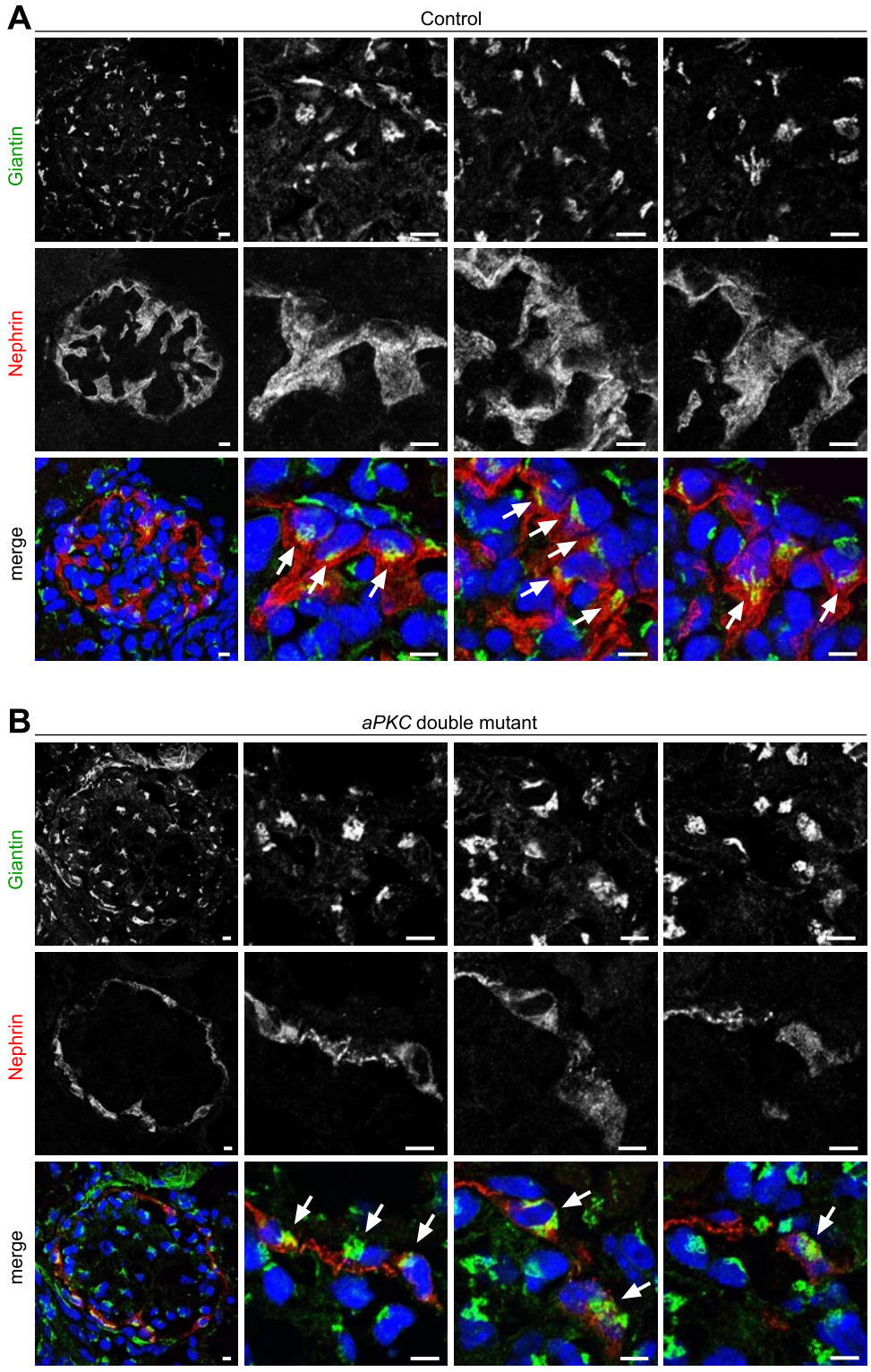

Supplemental Figure 8: Aberrant positioning of Golgi-apparatus in *aPKC* double knockout podocytes.

(A, B) Frozen kidney sections of control and *aPKC* double mutant mice at P4 were stained for the Golgi-apparatus marker Giantin and the podocyte marker Nephrin. While in control mice Golgi-apparatus (arrows) are restricted to the basal pole of the cytoplasm, in *aPKC* double knockout podocytes aberrant localization (arrows) can be detected. Scale bars: 5 µm.

Supplemental Figure 9

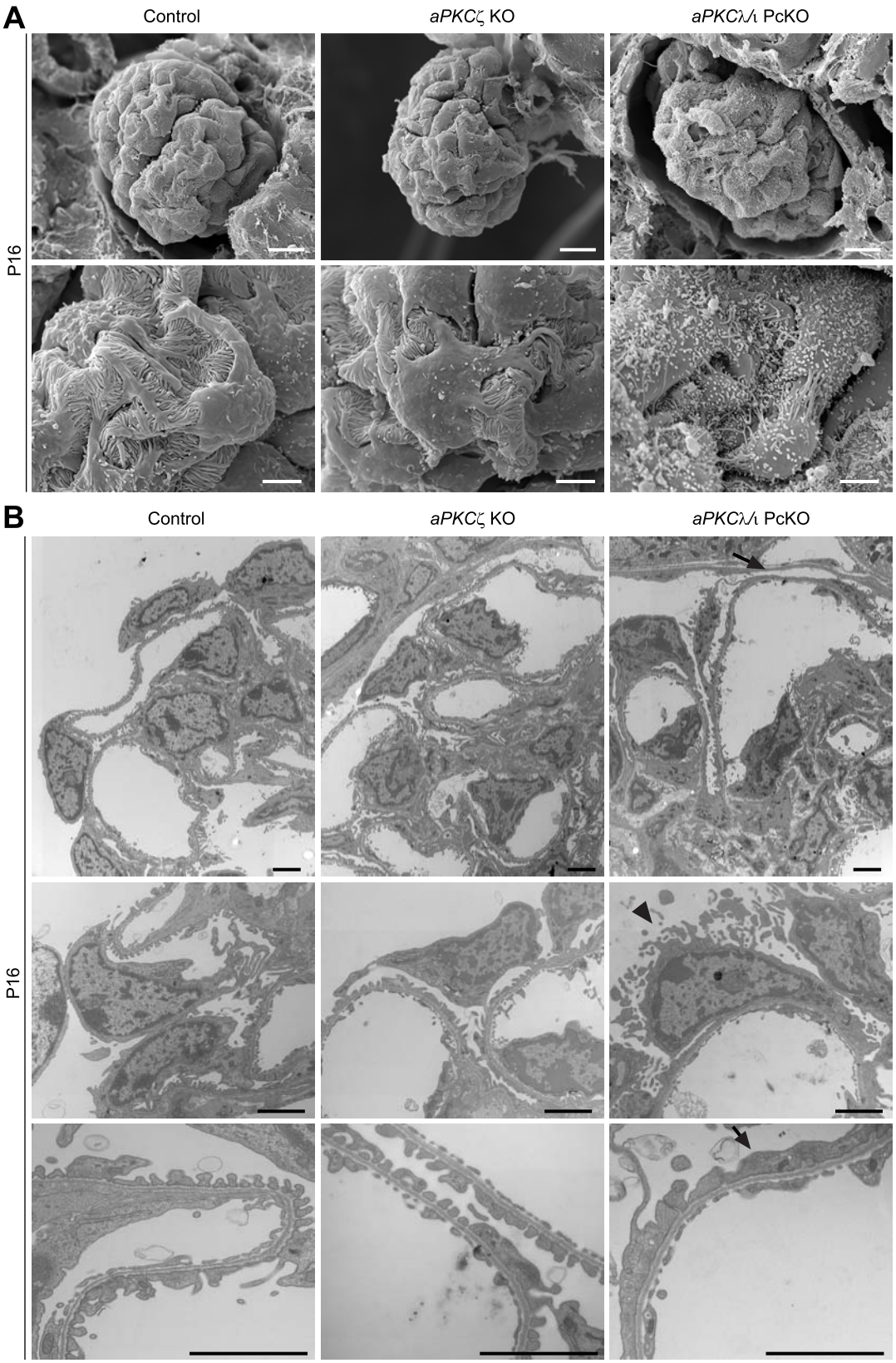

Supplemental Figure 9: Ultrastructural analysis of glomeruli at P16.

(A) Scanning electron micrographs show differentiated podocytes at P16. While podocytes of control and *aPKCζ* KO mice have regular primary processes and foot processes, the surface of *aPKCλ/ι* knockout podocytes is covered with microvilli, and no regular foot process network is detectable. **(B)** Transmission electron microscopy revealed foot process effacement (arrows) and podocyte microvilli and blebs (arrowhead) in *aPKCλ/ι* PcKO mice. Scale bars: 10 µm in A upper panel, 2.5 µm in A lower panel, 2 µm in B.